Progress In Electromagnetics Research C, Vol. 129, 173–186, 2023

Numerical and Measurement Based Modeling of a MiM Capacitor in a 0.25 µm SiGe-C BiCMOS Process

Huseyin Aniktar[1, *] and Huseyin S. Savci[1, 2]

Abstract—This study presents the generation of a scalable model based on measurement-aided numerical calculations for MiMCap (Metal-Insulator-Metal Capacitor) structures with a 0.25 µm SiGe-C BiCMOS technology. Various MiM capacitor structures with several different areas and peripheral sizes are fabricated in an in-house developed BiCMOS process. A set of fix-size models and a generic, scalable model are developed based on numerical EM calculations. The validity of the constructed model is verified with the measurement results. The model includes the breakdown voltage ratings, which are also extracted through the measurements. The model, EM simulations, and measurement results are in good agreement.

1. INTRODUCTION

Capacitors are one of the essential components in modern semiconductor processes. They are widely used in the design of integrated circuits as DC-block, bypass, decoupling, and matching elements. Among various types of capacitors, Metal-Insulator-Metal (MiM) (Metal-Insulator-Metal) capacitors have wide usage due to their ruggedness, availability of scalable models, and stable frequency characteristics. It is imperative to have an accurate MiM capacitor model for first-pass success in the design of integrated circuits [1–4].

Various custom-developed and commercial tools are available for capacitor modeling [5–8]. In this study, the MiM capacitors are modeled using Keysight's The Integrated Circuit Characterization and Analysis Program (IC-CAP) software [7]. Seven MiM structures are numerically simulated, measured, and modeled with IC-CAP. These structures are categorized as area dominant and peripheral-dominant. This approach proved the accuracy of the developed model over structural variety in sizes and shapes. The scalable model development is coded on Matlab.

There have been numerous studies on modeling MiM capacitors in the literature [9–13]. The methods used for modeling may vary, such as numerical and analytical approaches. Computer-aided design (CAD) tools are utilized to obtain single and scalable accurate models based on numerical EM calculations.

2. MIMCAP FABRICATION

The MiM capacitors are fabricated with 0.25 µm SiGeC BiCMOS (Silicon Germanium - Carbon Bipolar Complementary Metal Oxide Semiconductor) technology [14] with 1-poly and 5-metal layers. The technology stack-up is illustrated in Figure 1.

MiM structure is built between Metal4 and Metal3 layers, which are 0.03 µm thick and separated by 0.06 µm spacing.

Received 21 November 2022, Accepted 19 January 2023, Scheduled 2 February 2023

* Corresponding author: Huseyin Aniktar (aniktar@yahoo.com).

[1] Tubitak Bilgem, Semiconductor Test and Research Laboratory, Kocaeli, Turkey. [2] Istanbul Medipol University, Istanbul, Turkey.

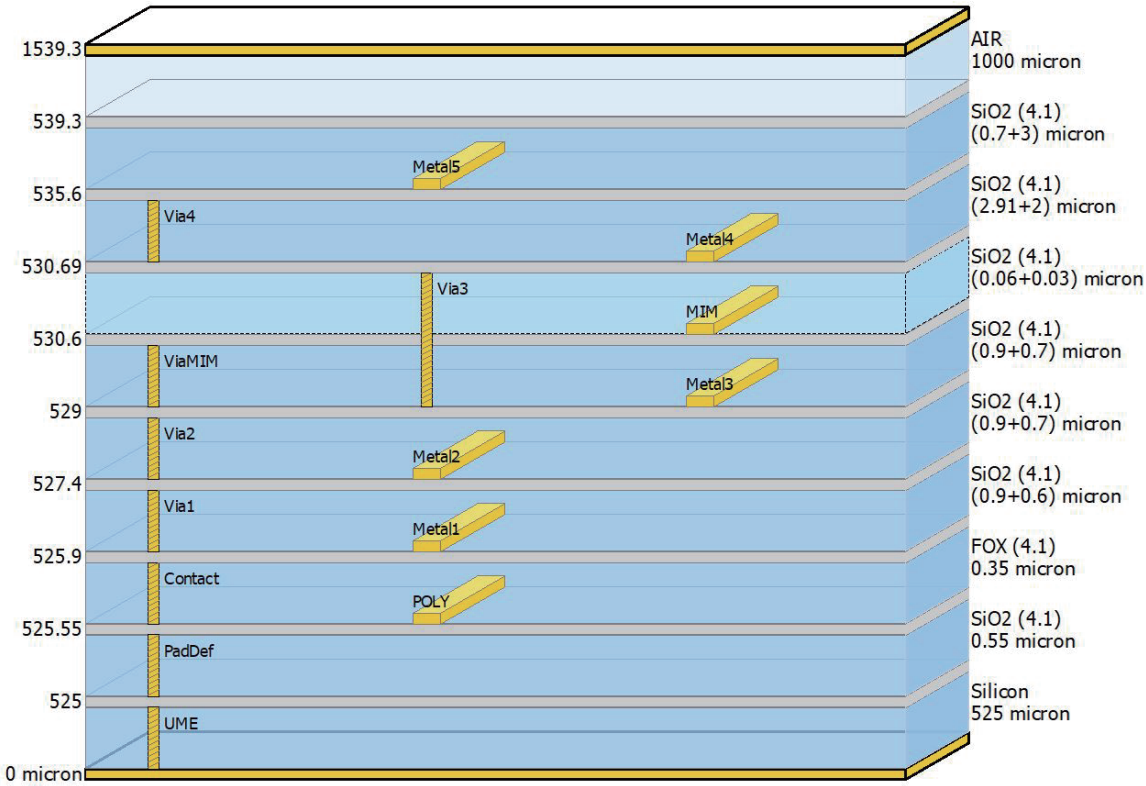

Figure 1. Stackup of 0.25 µm SiGeC BiCMOS technology.

The Metal-Insulator-Metal Capacitors (MiMCaps) are fabricated in various sizes such as 30 µm × 30 µm, 75 µm × 75 µm, 10 µm × 10 µm, 15 µm × 15 µm, 44.72 µm × 44.72 µm, 1.6 µm × 250 µm, and 4 µm × 250 µm. The sizes are selected to have different varieties of area and periphery sizes. Each plate of the capacitor is connected to Ground-Signal-Ground (GSG) pads with 50-ohm transmission lines. Short Open Load Through (SOLT) calibration structures with these launchers are also included for proper de-embedding. Figure 2 shows the layout of the MiMCap and an open launcher structure.

3. EM ANALYSIS

The measurement and numerical analyses of MiMCaps are used as an iterative process. The EM structure is constructed based on measured results. Once the target accuracy is obtained through EM simulation, the model generation is carried out. The numerical analysis is used to speed up the model process, and measurements are used to improve the accuracy of the EM setup [15, 16]. Figure 3 shows the EM view of M15, where numerical analyses are done.

Figures 4(a) and 4(b) show the input and output reflection coefficients for the M15 capacitor obtained from measurement results, EM analysis (20 cells/wavelength MoM), and generated model. As seen in the figure, they all show good agreement with each other.

For better comparison, EM solutions are done using methods such as MoM (Method of Moments) and FEM (Finite Element Method). The EM analyses are performed from 10 MHz to 27 GHz with 20 cells/wavelength mesh density in MoM, 100 cells/wavelength mesh density in MoM, and a mesh generated at the maximum frequency of 27 GHz in FEM. The results are compared with the measurement in Figure 5.

FEM EM simulations are closer to measurement results than MoM 20 cells/wavelength and 100 cells/wavelength. Simulation duration is 11 minutes 52 seconds for MoM 100, 11 minutes for MoM 20, and 12 minutes 30 seconds for FEM with Intel Core i7 7700 CPU @ 3.6 GHz 16 GB RAM machine.

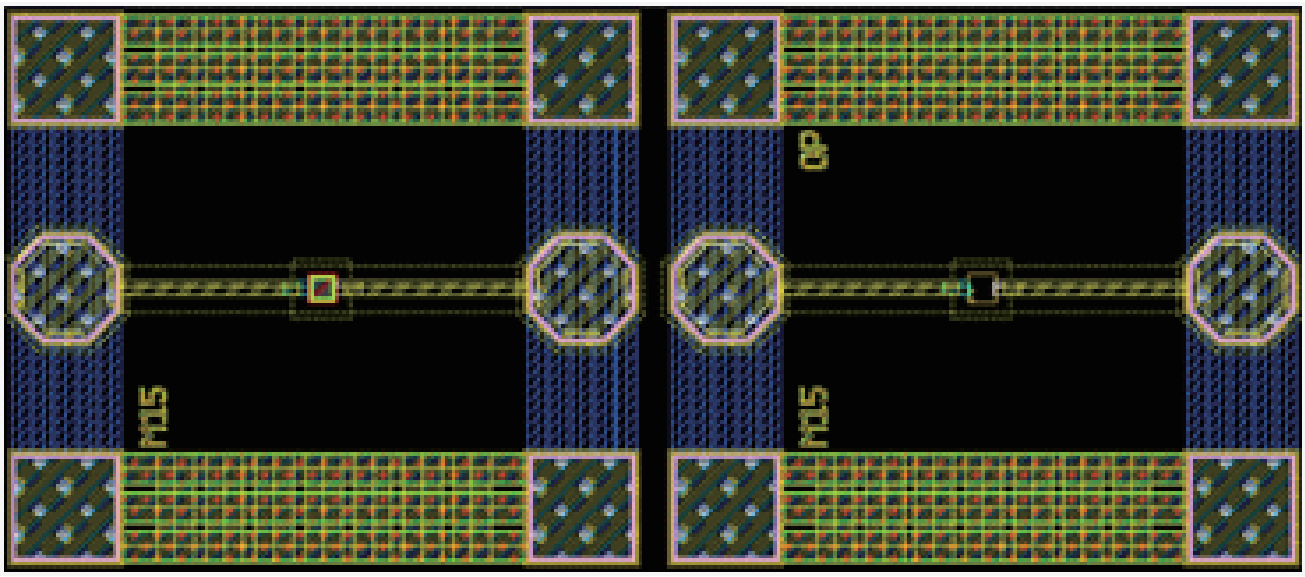

Figure 2. Layout of MiMCap test structure (a) and the launchers for fixture de-embedding (b).

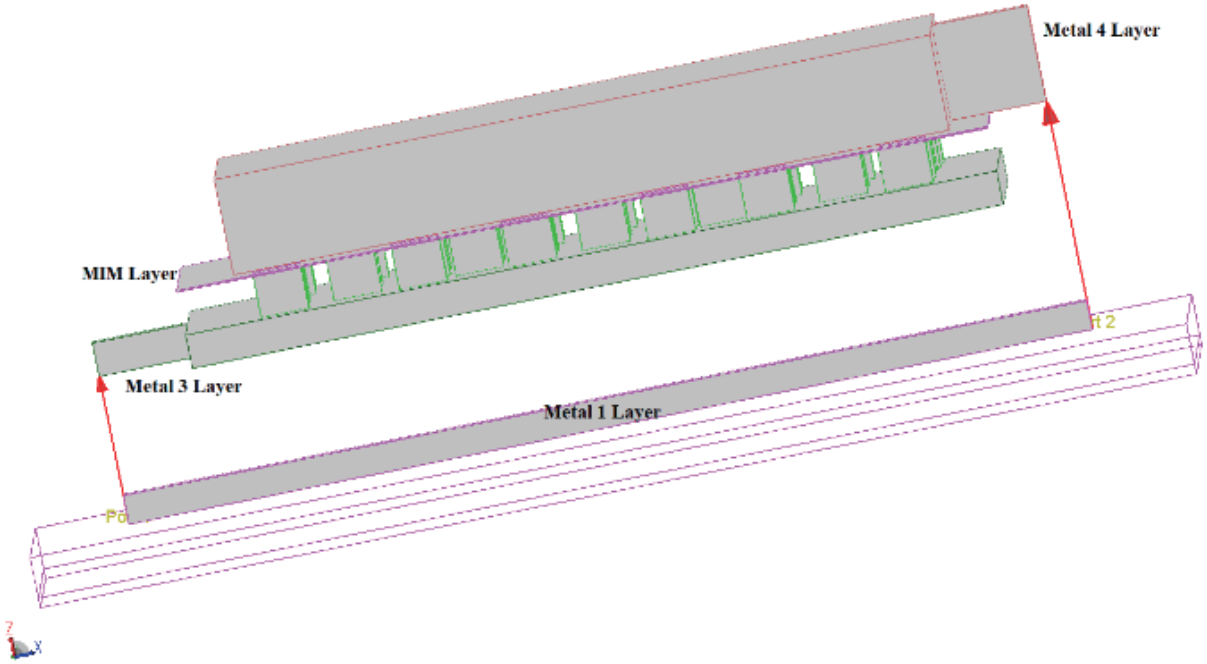

Figure 3. 15 µm × 15 µm (M15) layout for EM analysis.

4. MIMCAP MEASUREMENT AND DE-EMBEDDING

MiMCap measurements are done with an MPI probe station and N5222A PNA (performance network analyzer). Calibration is performed between 10 MHz and 26.5 GHz with 801 points, −33 dBm power, and 100 kHz Instantaneous Frequency (IF) Bandwidth (BW). Upon the probe-tip SOLT calibration on Impedance Standard Substrate (ISS), all capacitors, open and short test structures' S-parameters are measured. A two-step de-embedding procedure is applied to obtain the capacitor-only-measurement

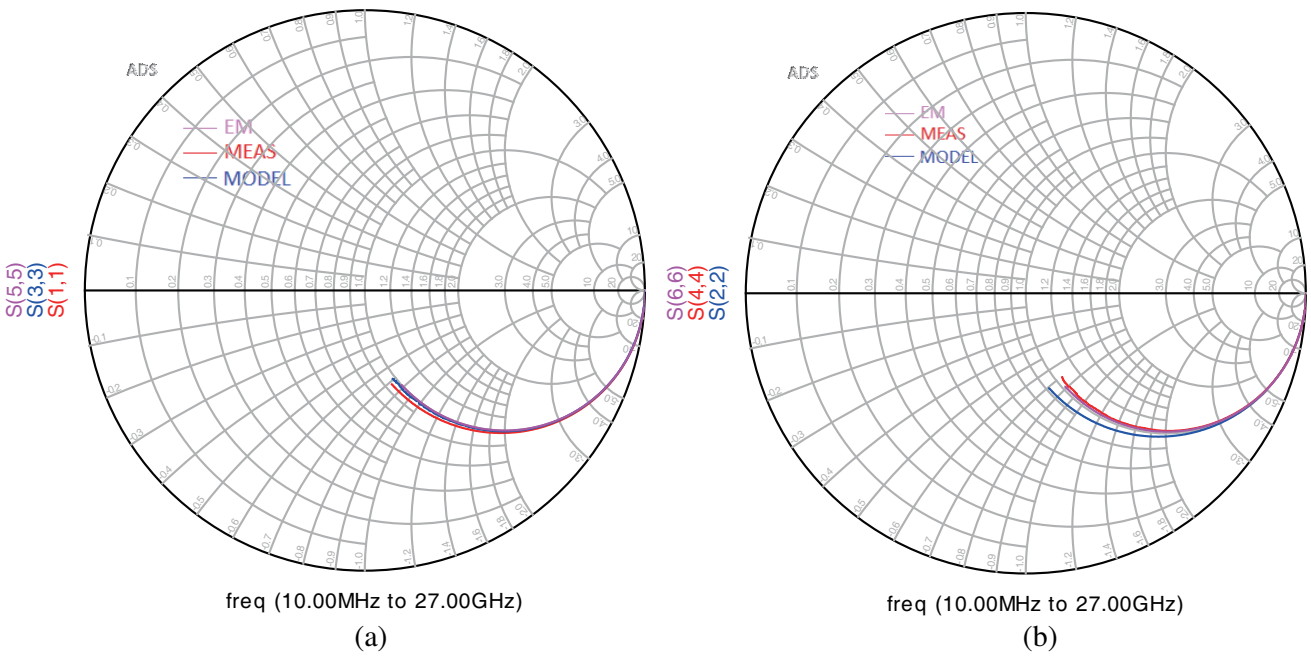

Figure 4. (a) Input. (b) Output reflection of M15 MiMCap measurement, model, and EM results.

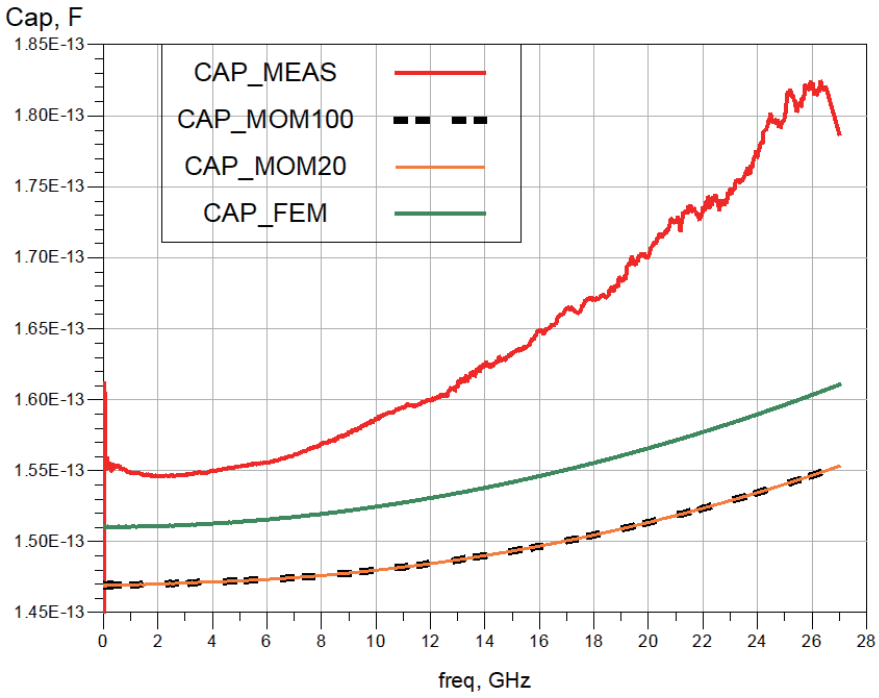

Figure 5. MiM 15 µm × 15 µm capacitance calculations based on measurements and various numerical methods.

results [17–19]. The processes of the two-step de-embedding technique are as follows:

- Measure the S-parameters (Stest_structure, Sopen, Sshort). Convert them to Y-parameters (Ytest_structure, Yopen, Yshort).
- Perform the first step of de-embedding by removing the parallel parasitics from both Ytest_structure and Yshort according to the following Equations (1) and (2):

$$Y_{test\_structure1} = Y_{test\_structure} - Y_{open} \quad (1)$$

$$Y_{short1} = Y_{short} - Y_{open} \quad (2)$$

- Perform the second de-embedding by removing the series parasitics. Obtain Zshort1 from Yshort1, and Ztest_structure1 from Ytest_structure1. Calculate Zcomponent as shown in Equation (3).

$$Z_{component} = Z_{test\_structure1} - Z_{short1} \quad (3)$$

Zcomponent is the de-embedded data corresponding to the measured data. A MATLAB routine is generated as follows;

$mk11$ = sparameters ('MIMcap.s2p');
$mk12$ = sparameters ('MIMopen.s2p');
$mk13$ = sparameters ('MIMshort.s2p');
$Ydut$ = yparameters ($mk11$);
$Yopen$ = yparameters ($mk12$);
$Yshort$ = yparameters ($mk13$);
$Ydut1$ = Ydut.Parameters-Yopen.Parameters;
$Yshort1$ = Yshort.Parameters-Yopen.Parameters;
$Zdut1 = y2z$ (Ydut1);
$Zshort1 = y2z$ (Yshort1);
$Zcomp = Zdut1 - Zshort1$;
Ydutdembedded = $z2y$ (Zcomp);
Sdutdembedded = $z2s$ (Zcomp);
freq = $mk11$. Frequencies;
rfwrite (Sdutdembedded, freq, 'MIMcap_deembed.s2p')

Figure 6 shows the de-embedded data and raw data on Smith charts. The de-embedded data reveals the true characteristic of capacitors for which the EM simulations are compared, and the models would be constructed.

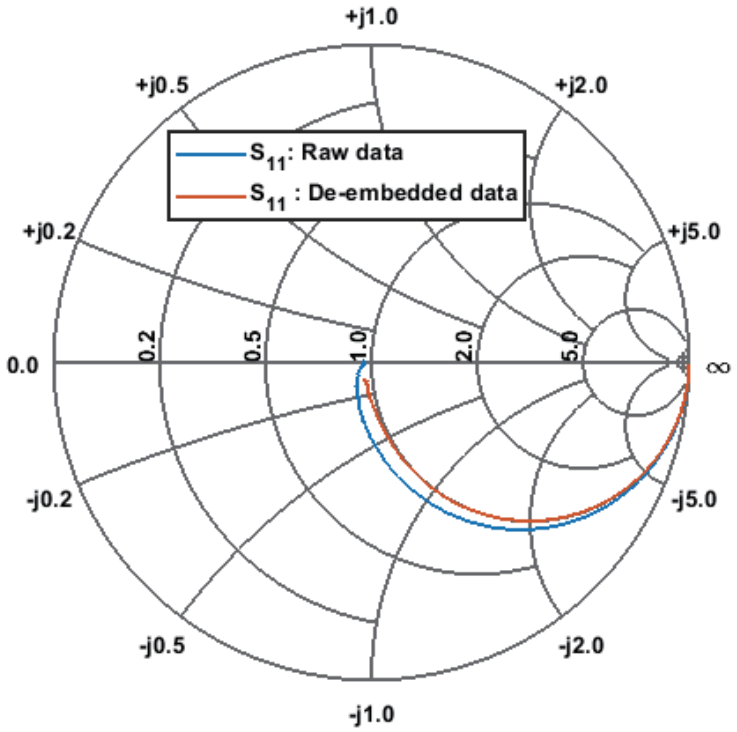

Figure 6. De-embedded and raw data illustration.

5. MIMCAP MODELLING

The modeling routines are written using IC-CAP [20]. Several circuit topologies and modeling routines are investigated in the literature [21–26]. The circuit topology used for model fitting is presented in Figure 7. Here $C12$ stands for the total ideal capacitor value due to parallel plate and fringing field effects. $R12$ and $CpR12$ represent Effective Series Resistance and its deviation across the frequency band. $L12$ is for the parasitic inductance due to metal connections which set the value of the capacitor's Self Resonance Frequency. $CpR10/20$ and $R10/20$ represent the parasitics due to substrate coupling distributed over the input and output terminals of the capacitor. Both single and scalable models are generated.

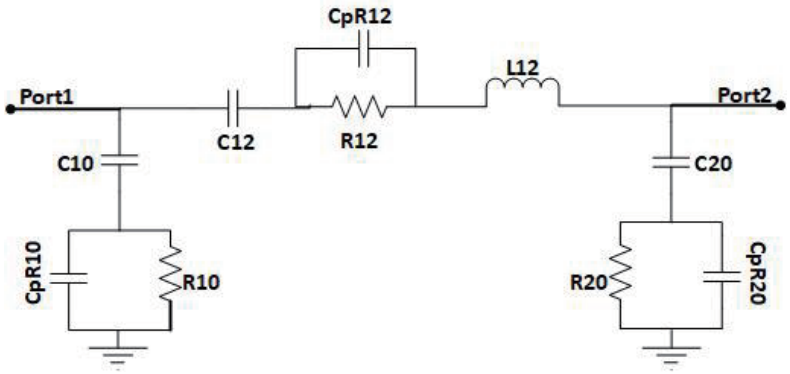

Figure 7. Circuit topology used for MiMCap modeling.

5.1. Single MiMCap Model

This section presents the modeling procedure for a fixed size, 15 µm × 15 µm MiMCap. The procedure covers the parameter extraction for each component value of the circuit topology shown in Figure 7 based on the data, which is the fusion of numerical EM solutions and measurement results. Here the term fusion is adopted to represent the iterative process for the high level of agreement between measured and simulated results. The EM numerical model matches measured performance by optimizing the EM stack-up and material electrical properties. On the other hand, the measurement procedure is optimized to ensure a repeatable measurement, an accurate calibration, and a proper de-embedding of launcher structures to obtain the correct response of capacitors right at the simulated plane. The VNA settings, such as resolution bandwidth, and probe station settings, such as proper shielding, were also part of the measurement optimization procedure. The input reflection and the forward transfer coefficient of both model and measurements are shown in Figures 8(a) and 8(b). The Root Mean Square (RMS) errors between the model performance and measurement results are 3.7% for S_{21} and 12.96% for S_{11}.

Table 1. Extracted parameters for M15 MiMCap.

Parameter	Value
$C10$ & $C20$	5 fF & 15 fF
$R10$ & $R20$	300 ohm & 1.5 Kohm
$CPR10$ & $CPR20$	856 aF & 14 fF
$C12$	145 fF
$R12$	4.25 ohm
$CPR12$	1.96 pF
$L12$	92 pF

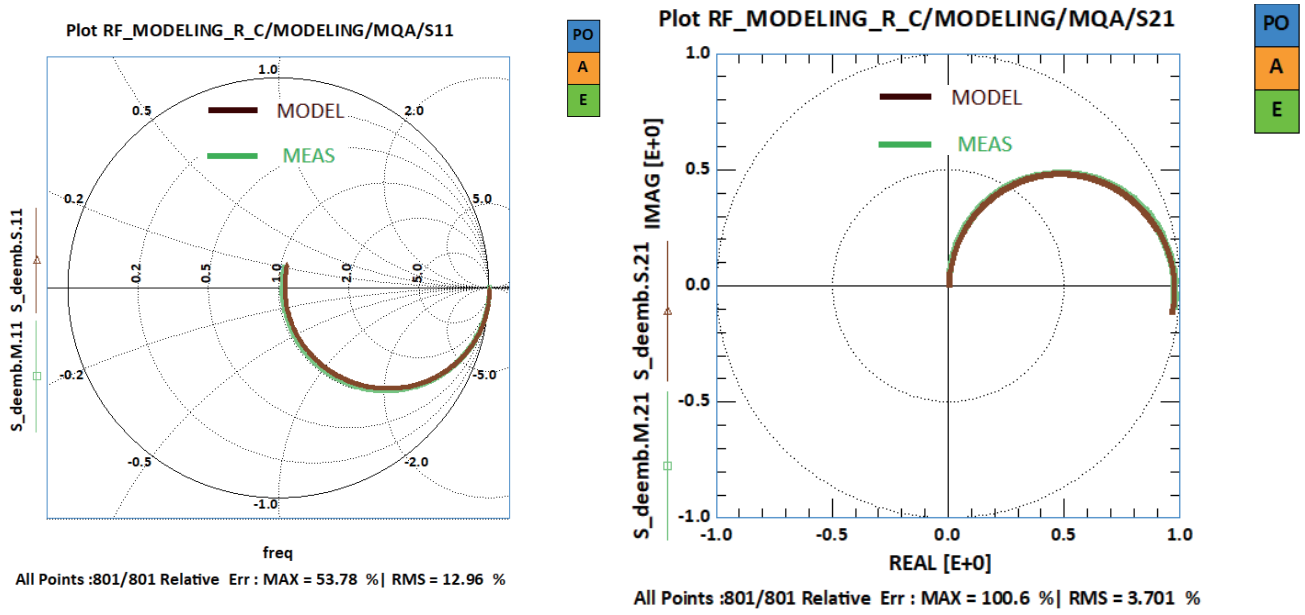

Figure 8. (a) S_{11} (b) S_{21} model and measurement.

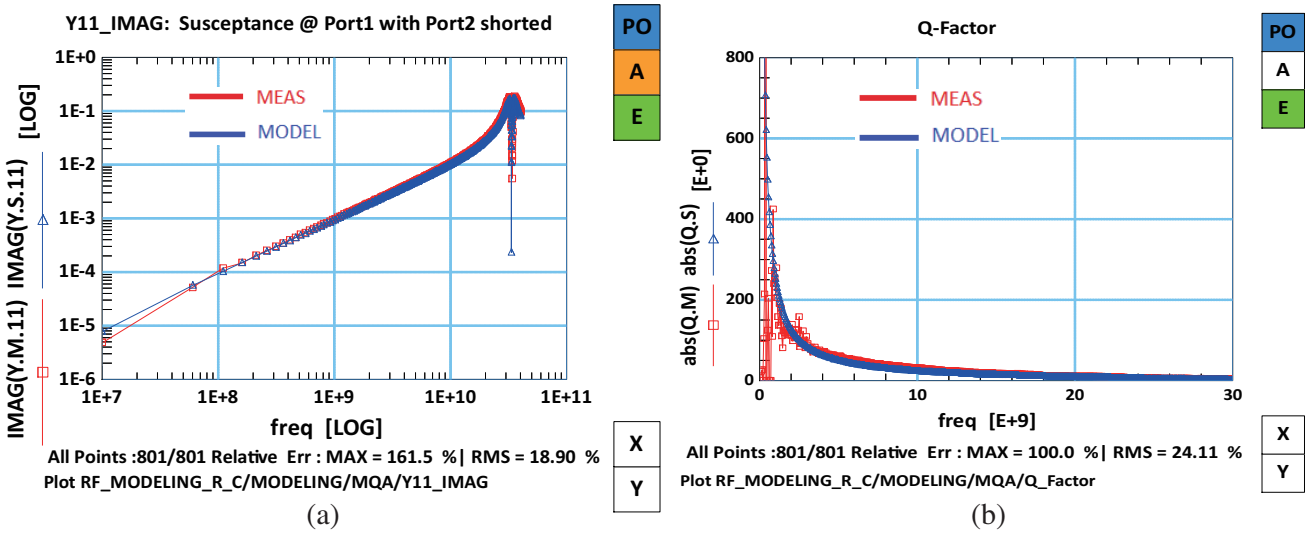

Figure 9. (a) Y11 model and measurement, (b) Q-factor model and measurement.

Figure 9 shows the input admittance and Q-factor of modeled and measured performance of fix size capacitor. Here, RMS errors between model (Y.S.11) and measurement (Y.M.11) are 18.9% for Y11 imaginary and 24.11% for Q factor, respectively. The extracted parameters for fix-size capacitors are given in Table 1.

5.2. Scalable MiMCap Model

The scalable model is generated from a set of fixed-size models. Once the models for several different-sized caps are obtained, all values are plotted versus the corresponding size parameters. These values versus parameters form a curve. A proper polynomial is fit to this curve using MATLAB. The new circuit is a scalable cap model, where the component values are a function of the design parameters,

Table 2. Scalable model parameters.

Parameter	Value
$C10$	$1.126 \times 10^{-14} - 5.048 \times 10^{-10} \times w - 5.976 \times 10^{-11} \times l$ $+1.76 \times 10^{-6} \times w^2 + 9.69 \times 10^{-6} \times w\times$
$R10$	300 ohm
$CPR10$	$-4.675 \times 10^{-15} + 7.587 \times 10^{-10} \times w + 3.357 \times 10^{-11} \times l$ $-2.868 \times 10^{-6} \times w^2 - 6.503 \times 10^{-6} \times w \times l$
$C12$	$-6.334 \times 10^{-15} - 3.283 \times 10^{-10} \times w + 1.255 \times 10^{-10} \times l$ $+1.795 \times 10^{-6} \times w^2 + 0.0006654 \times w \times l$
$R12$	$2.987 - 2.968 \times 10^4 \times w + 2541 \times l$ $+1.274 \times 10^8 \times w^2 - 4.97 \times 10^7 \times w \times l$
$CPR12$	$2.298 \times 10^{-12} + 5.629 \times 10^{-8} \times w - 7.594 \times 10^{-9} \times l$ $-0.0002526 \times w^2 - 0.0001696 \times w \times l$
$L12$	$8.836 \times 10^{-11} - 1.92 \times 10^{-6} \times w - 5.184 \times 10^{-8} \times l$ $+0.0007389 \times w^2 + 0.005471 \times w \times l$
$C20$	15 fF
$R20$	1.5 Kohm
$CPR20$	14 fF

such as width and length. The scalable capacitor model is valid only within the specific range of design parameters. Table 2 shows the list of parameters where w is the width in μm, and l is the length in μm. The range of measurement is specified based on the following cap sizes: 30 μm × 30 μm, 75 μm × 75 μm, 10 μm × 10 μm, 15 μm × 15 μm, 44.72 μm × 44.72 μm, 1.6 μm × 250 μm, 4 μm × 250 μm.

For each capacitor, the capacitance value of the scalable model and measured results at 100 MHz and 10 GHz are listed in Table 3 (in fF). The frequency performance of the scalable model and measurement results for the capacitor M15 are plotted in Figure 10.

Table 3. Measurement and scalable model comparison.

		100 MHz		10 GHz	
	Size	Meas. (fF)	Model (fF)	Meas. (fF)	Model (fF)
$MK1$	$(30\,\mu m)^2$	580.4	588.7	601.5	618.8
$MK2$	$(75\,\mu m)^2$	3494	3764	3353	3580
$MK3$	$(10\,\mu m)^2$	79.06	85.29	75.23	79.47
$MK9$	1.6 μm × 250 μm	286.9	330	312.6	348.7
$MK11$	4 μm × 250 μm	678.2	625	805.4	736.5
$M15$	$(15\,\mu m)^2$	151.2	158.8	155.5	155.7
$M19$	$(44.72\,\mu m)^2$	1250	1316	1385	1405

5.3. Area and Perimeter Capacitance

Area and perimeter capacitance values are calculated according to Equations (4) and (5).

$$C1 = A1 \times CA + P1 \times CP \tag{4}$$

$$C2 = A2 \times CA + P2 \times CP \tag{5}$$

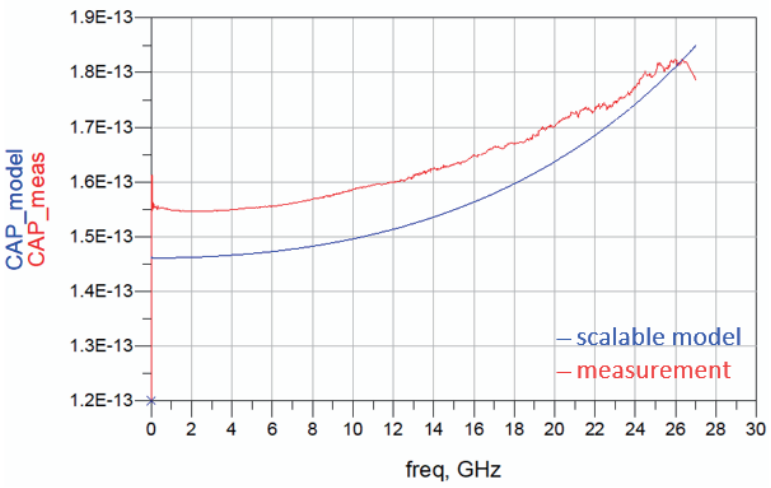

Figure 10. 15 µm × 15 µm MiMCap scalable model and measurement.

CA is the area capacitance; CP is the perimeter capacitance; $C1$ is the capacitance value at the specified frequency; $A1$ is the area of $C1$; $P1$ is the perimeter of $C1$; $C2$ is the capacitance value at the specified frequency; $A2$ is the area of $C2$; and $P2$ is the perimeter of $C2$. The calculations are performed in Table 4 for different frequencies.

Table 4. $MK2$ and $MK9$ area-perimeter cap calculation.

	100 MHz	10 GHz	20 GHz
$MK2$	3.49 pF	3.35 pF	3.06 pF
$MK9$	286.9 fF	312.6 fF	443.1 fF
CA [fF/µm^2]	0.6162	0.5873	0.5190
CP [fF/µm]	0.0804	0.1544	0.4680
Ctotal $= CA + CP$	0.6966	0.7447	0.987

Table 4 shows that perimeter capacitance increases by frequency while the area capacitance decreases. Area capacitance CA is 0.6162 fF/µm^2, and perimeter capacitance Cp is 0.0804 fF/µm^2 at 100 MHz. When the frequency increases to 20 GHz, the perimeter capacitance increases to 0.4680 fF/µm^2, and area capacitance decreases to 0.5190 fF/µm^2. In the table, there is one more parameter, Ctotal, which is described as follows;

$$C_{total} = \left(CA \times 1\,\mu m^2\right) + \left(CP \times 1\,\mu m\right) \tag{6}$$

5.4. Breakdown Voltage Measurement

The breakdown voltage for a capacitor is the highest voltage that the insulator can withstand the electrical field without an irreversible dielectric punch-through due to an excessive electric field. The breakdown voltage measurement is a destructive procedure. The voltage across the capacitor is swept, and the current is monitored. Once the voltage exceeds the breakdown, the dielectric between the plates is no longer an insulator, and electrons start moving from one plate to the other, generating a current flow. Figure 11 shows the monitored current for a 15 µm × 15 µm MiM capacitor. It is evident that the breakdown happens at around 32 V, and then the current starts to pass flow. Here current limit of the supply is set to a finite value to prevent further damage. The breakdown is an irreversible damage mechanism. Figure 12 shows the current-voltage relationship of $M15$ after the part is exposed to voltages beyond the breakdown point. Figure 13(a) shows the 15 µm × 15 µm MiMCap ($M15$) photo, and Figure 13(b) shows the MiM photo after the breakdown.

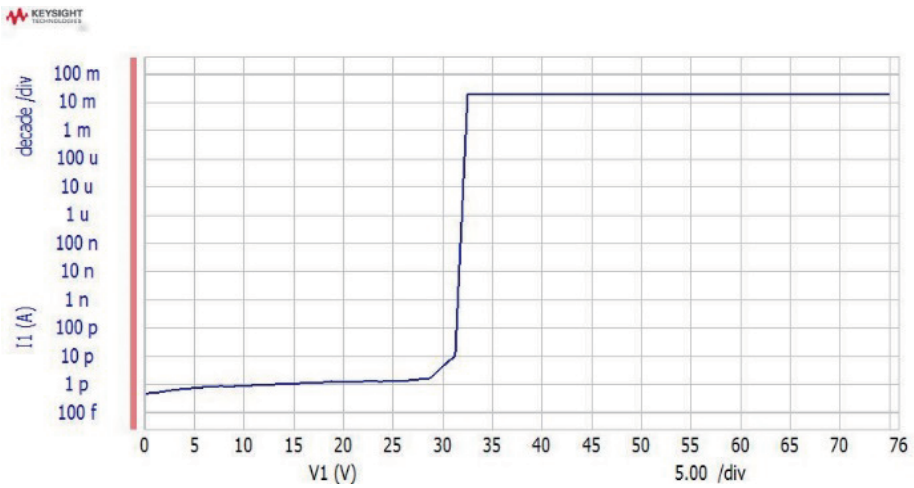

Figure 11. Voltage sweep on $M15$.

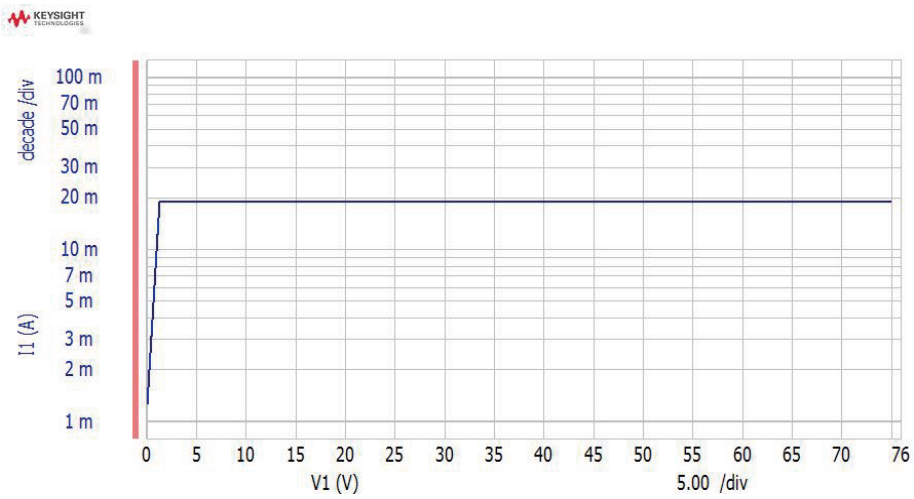

Figure 12. I-V characteristic of $M15$ after the breakdown.

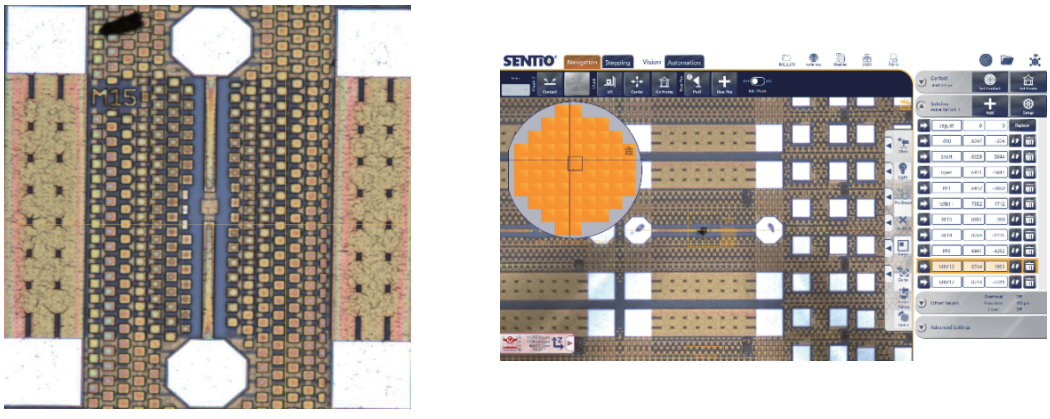

(a) (b)

Figure 13. (a) MiM 15 µm × 15 µm photo (b) after the breakdown.

According to JESD35-A standards [27], the maximum voltage limit for MiM capacitance is $V_{\max}$. This limit is specified at 30 MV/cm for oxides less than 20 nm thick and 15 MV/cm for thicker oxides.

Based on the voltage sweep in Figure 11, the capacitance breakdown voltage is found as 32 V. Process oxide thickness is 60 nm, then MiM capacitance electric field strength can be calculated using Equation (7). From 32 V = 60 nm $\times$ V_{mim}, the electrical field strength is calculated as 5.33 MV/cm.

$$V_{\max} = V_{mim} \times tox \tag{7}$$

5.5. Temperature Model

The $M15$ capacitor is measured at various temperatures, such as 85°C, 25°C, and −40°C, to generate a temperature-dependent model. Capacitance measurements are performed at 1 MHz, 50 mV AC voltage, and −3 V to +3 V DC sweep with B1500A CMU. Figure 14 shows the normalized capacitance measurements −40°C and +85°C for the values at 25°C.

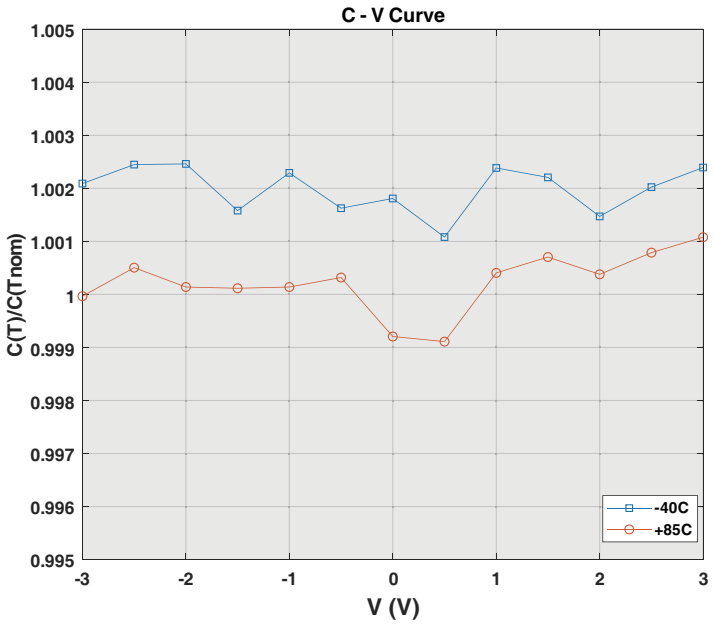

Figure 14. $M15$ normalized cap values at −40°C & +85°C.

The temperature-dependent capacitor value is given in Equation (8).

$$C\left(T\right) = C\left(T_{nom}\right) \times \left[1 + TC1 \times dT + TC2 \times dT^2\right] \tag{8}$$

$C(T)$ is the capacitance value for each temperature; $dT = T - Tnom$ ($Tnom$ is 25°C nominal temperature); $TC1$ and $TC2$ temperature constants. Using the measured capacitance values at 85°C and −40°C and Equation (8), we find the temperature constants $TC1$ as -3.084×10^{-4} and $TC2$ as 5.18×10^{-6}. In the MiMCap model, temperature dominantly affects the main capacitance $C12$. We can apply the temperature effect to the MiMCap model as follows:

$$C12 \times [1 + TC1 \times dT + TC2 \times dT^2] \tag{9}$$

5.6. Corner Model

To extract the process corner variations, $M15$ capacitors are measured on 60 different locations of wafers. A statistical distribution is obtained as follows:

typical_mim
sigma_cap = 0
mim_factor = 1 − 0.100∗ sigma_cap/3

fast_mim
sigma_cap = 0.9
mim_factor = $1 - 0.100*$ sigma_cap/3
slow_mim
sigma_cap = -0.9
mim_factor = $1 - 0.100*$ sigma_cap/3

The corner model dominantly affects the main capacitance $C12$ and resistance $R12$. The corner effect can be applied as follows:

$C12 * [1 + TC1 * dT + TC2 * dT^2] *$ mim_factor
$R12 *$ mim_factor

Table 5 compares the MiMCap modeling performance to those previously reported in the literature.

Table 5. Comparison with previously published MiMCap models.

Process	Freq.	CAP size	CAP Value	EM Solver	Breakdown Included	Scalable Model	CAD Tool	Meas.	Ref.
0.25 µm SiGe BiCMOS	10 GHz 110 GHz	250µm^2 4900µm^2	250 fF 4.9 pF	SONNET	No	No	Agilent ADS	Yes	[3]
0.18 µm Bulk-Si	2 GHz 6 GHz	-		No	No	No	Spice & ICCAP	Yes	[8]
GaAs	1 GHz–20 GHz	2560 µm^2 19400 µm^2	0.4 pF 15 pF	Not Specified	No	Yes	Not Specified	Yes	[12]
0.25 µm SiGe BiCMOS	10 MHz 110 GHz	49 µm^2 1800 µm^2	50 fF 4.9 pF	Agilent ADS	No	Yes	Agilent ADS	Yes	[25]
0.25 µm SiGe BiCMOS	10 MHz 27 GHz	100 µm^2 2000 µm^2	80 fF 1.3 pF	MOM & FEM	Yes	Yes	ICCAP	Yes	This work

Table 5 presents the comparison with previously published MiMCap models. The MiMCap analytical model should agree on both EM and measurement results. In the table, the prior published works are listed with details such as frequency coverage, breakdown consideration, the name of CAD tools for optimization and modeling, the EM solvers for the analysis, and the involvement of measurement. This work comes forward among tabulated ones as it reports the breakdown voltage. The breakdown voltage effect is characterized through the measurements but not included in the model yet. The temperature dependence and breakdown voltage effect will be included in the evolved versions of the model.

6. CONCLUSION

This study explains the model generation steps of a Metal-Insulator-Metal capacitor in in-house developed 0.25 µm SiGe-C BiCMOS process. The procedure and methodology of temperature and corner-dependent scalable model are described in detail. The generated models show good agreement with numerical analysis and measurement results.

REFERENCES

1. Daly, D. A., S. P. Knight, M. Caulton, and R. Ekholdt, "Lumped elements in microwave integrated circuits," *IEEE Trans. Microwave Theory and Tech.*, Vol. 15, 713–721, Dec. 1967.

2. Robertson, I. D. and S. Lucyszyn, *RFIC and MMIC Design and Technology*, 3rd Edition, 83–116, EPSRC Publication, US, 1998.
3. Gruner, D., Z. Zhang, V. Subramanian, F. Korndoerfer, and G. Boeck, "Lumped element MIM capacitor model for Si-RFICs," *Int. Microwave & Optoelectronics Conference (IMOC)*, Brazil, Oct. 29–Nov. 1, 2007.
4. Jamal Deen, M. and T. A. Fjeldly, "CMOS RF modeling, characterization and applications," *World Scientific*, 2002.
5. Zhang, L. and P. H. Aaen, "Automatic modeling of passive components for RFIC circuit design using sonnetlab," *29th Annual Review of progress in Applied Computational Electromagnetics*, Canada, Mar. 24–28, 2013.
6. Zhang, L. and S. Arvas, "Automatic model extraction for RFIC spiral inductors using sonnetLab," *30th Annual Review of Progress in Applied Computational Electromagnetics*, FL, USA, Mar. 23–27, 2014.
7. Keysight, *PathWave Device Modeling: IC-CAP (Integrated Circuit Characterization and Analysis Program)*, 2021.
8. Agarwal, S., S. Raut, H. S. Jatana, A. Dixit, and S. Chatterjee, "SPICE based compact modeling of spiral inductor and MIM capacitor for RF circuit simulations," *5th Int. Conference on Emerging Electronics (ICEE)*, India, Nov. 26–28, 2020.
9. Chew, W. C. and L. J. Jiang, "A complete variational method for capacitance extractions," *Progress In Electromagnetics Research*, Vol. 56, 19–32, 2006.
10. Mellberg, A. and J. Stenarson, "An evaluation of three simple, scalable MIM capacitor model," *IEEE, MTT-S*, Vol. 54, No. 1, 169–172, Jan. 2006.
11. Mondal, J., "An experimental verification of a simple distributed model of MIM capacitors for MMIC applications," *IEEE MTT-S*, Vol. 34, No. 4, 403–408, Apr. 1987.
12. Wang, L., R. M. Xu, and B. Yan, "MIM capacitor simple scalable model determination for MMIC application on GaAs," *Progress In Electromagnetics Research*, Vol. 66, 173–178, 2006.
13. Sanusi, R., K. Norhapizin, S. A. E. Ab Rahim, A. I. Ab Rahim, A. Marzuki, and M. Yahya, "Scalable MIM capacitor polynomial equation model development with application in the design of 2.4 GHz PHEMT low noise amplifier," *Asia Pacific Microwave Conference*, Singapore, Dec. 2009.
14. Racanelli, M., S. Voinegescu, and P. Kempf, "High-performance SiGe BiCMOS technology," *ACES Conference*, HI, USA, 2005.
15. Beere Sha R. S., A. M. Khan, and H. V. Manjınath Reddy, "Design and EM-simulation of MIM capacitor," *Int. Conference on Energy, Communication, Data Analytics and Soft Computing (ICECDS)*, India, Aug. 1–2, 2017.
16. Gerhard, G. and S. Koch, "MIM shunt-capacitor model using black boxes of EM-simulated critical parts," *IEEE Trans. MTT*, Vol. 49, No. 3, 559–562, Mar. 2001.
17. Mangan, A. M. and S. P. Voinigescu, Ming-Ta Yang and Mihai Tazlauanu, "De-embedding transmission line measurements for accurate modeling of IC designs," *IEEE Trans. on Electron Devices*, Vol. 53, 235–241, Feb. 2006.
18. Schroder, D. K.. *Semiconductor Material and Device Characterization*, Wiley & Sons, 3rd Edition, 2006.
19. Jordan, L., D. Elsherbeni, E. Hutchcraft, R. K. Gordon, and D. Kajfez, "On-wafer measurement and modeling of silicon carbide MESFET's," *ACES Journal*, Vol. 23, No. 1, Mar. 2008.
20. Sischka, F., *IC-CAP Modeling Handbook*, *Agilent Technologies*, Oct. 2010.
21. Lombard, P., J.-D. Arnould, O. Exshaw, H. Eusebe, P. Benech, A. Farcy, and J. Torres, "MIM capacitors model determination and analysis of parameter influence," *Int. Symposium on Industrial Electronics, ISIE*, Croatia, Jun. 2005.
22. Jeyaraman, S., V. N. R. Vanukuru, D. Nair, and A. Chakravorty, "Modeling of high-Q conical inductors and MOM capacitors for milimeter-wave applications," *IEEE Transactions on Electron Devices*, Vol. 67, No. 12, Dec. 2020.

23. Zhang, R., Q. Zhang, X. Zhou, y. Zhu, X. Ming, and N. Gao, "Design and fabrication of the silicon-based integrated MIM capacitors," *19th Int. Conference on Electronic Packaging Technology (ICEPT)*, China, Aug. 8–11, 2018.
24. Hourdakis, E., A. Travlos, and A. G. Nassiopoulou, "High-performance MIM capacitors with nanomodulated electrode surface," *IEEE Transactions on Electron Devices*, Vol. 62, No. 5, 2015.
25. Korndörfer, F. and V. Mühlhaus, "Lumped modeling of integrated MIM capacitors for RF applications," *88th ARFTG Microwave Measurement Conference*, TX, USA, Dec. 8–9, 2016.
26. Yi, C., Y. Lu, H. Zhang, Z. Zhao, X. Ma, and Y. Hao, "A novel scalable series MIM capacitor model for MMIC applications," *16th China Int. Forum on Solid State Lighting*, China, Nov. 25–27, 2019.
27. JEDEC, *Procedure for Wafer-Level-Testing of Thin Dielectrics: JESD35-A*, Apr. 2001.